12

# CALCULATION OF THE LONGITUDINAL AERODYNAMIC CHARACTERISTICS OF WING-FLAP CONFIGURATIONS WITH EXTERNALLY BLOWN FLAPS*

Michael R. Mendenhall
Nielsen Engineering & Research, Inc.

## SUMMARY

An analytical method for predicting the longitudinal aerodynamic characteristics of externally blown flap configurations is described. Two potential flow models make up the prediction method: a wing and flap lifting-surface model and a turbofan engine wake model. A vortex-lattice lifting-surface method is used to represent the wing and multiple-slotted trailing-edge flaps. The jet wake is represented by a series of closely spaced vortex rings normal to a centerline which is free to move to conform to the local flow field. The two potential models are combined in an iterative fashion to predict the jet wake interference effects on a typical EBF configuration. Comparisons of measured and predicted span-load distributions, individual surface forces, forces and moments on the complete configuration, and flow fields are included.

## INTRODUCTION

The short take-off and landing requirements for STOL aircraft necessitate a means of achieving very high lift coefficients on aircraft in take-off or landing configuration with little sacrifice in cruise performance. The externally blown jet-augmented flap (EBF) provides such a means. The jet efflux from engines mounted beneath the wing is allowed to impinge directly on the slotted flap system (fig. 1), thus producing a large amount of additional lift through engine wake deflection and mutual interference effects.

An analytical method for predicting the longitudinal aerodynamic characteristics of EBF configurations has been developed (ref. 1). Potential flow models of the lifting surfaces and the jet wake are combined in an iterative fashion to satisfy two requirements. First, the tangency boundary condition must be satisfied at selected points on each lifting surface, and second, the centerline of each jet wake must lie along a streamline of the total flow field. One goal of the EBF method is to predict

*Sponsored by NASA Langley Research Center, Contract NAS1-13158.

the total loads and distribution of loads on each component of the wing-flap configuration under the influence of multiple jet wakes. A second goal is that a minimum of empirical information be required as input to the method.

This paper contains a discussion of the technical approach to the prediction of EBF aerodynamic characteristics, a discussion of the development of the potential flow models, and some comparisons with data.

## SYMBOLS

| | |
|---|---|
| $c_n$ | section normal-force coefficient |
| $C_D$ | drag coefficient, positive aft |
| $C_L$ | lift coefficient |
| $C_m$ | pitching-moment coefficient, positive nose up |
| $C_N$ | normal-force coefficient |
| $C_T$ | thrust coefficient of a single jet |
| $C_\mu$ | total thrust coefficient for a configuration with multiple jets |
| R | local radius of circular jet, m (ft.) |
| $R_o$ | initial radius of circular jet, m (ft.) |
| u | axial velocity, m/sec (ft/sec) |
| V | free-stream velocity, m/sec (ft/sec) |
| $V_j$ | initial jet wake velocity, m/sec (ft/sec) |
| $x_j,y_j,z_j$ | jet coordinate system with origin at the center of the jet inlet |
| X,Y,Z | wing coordinate system with origin at the wing root chord leading edge |
| $\alpha$ | angle of attack, degrees |
| $\gamma$ | jet wake vortex cylinder strength, m/sec (ft/sec) |
| $\delta_f$ | flap deflection angle, degrees |

| | |
|---|---|
| $\Delta$ | convergence tolerance |
| $\Delta s$ | jet model vortex ring spacing, m (ft.) |
| $\eta$ | dimensionless spanwise coordinate |
| $\phi$ | dihedral angle, degrees |

## ANALYSIS

### Wing-Flap Vortex-Lattice Model

The lifting surfaces of externally blown flap configurations consist of a wing and multiple-slotted trailing-edge flaps. The lifting-surface model needed to represent the typical EBF wing-flap configuration must be capable of handling individual lifting surfaces and predicting the spanwise and chordwise load distributions on each surface. Mutual interference between surfaces must be considered along with interference effects induced by some external source of disturbance, for example, the wake of a high bypass ratio turbojet engine. It is also essential that the lifting-surface model be capable of predicting the velocity field induced in the vicinity of the wing and flaps. The above requirements are best fulfilled through the use of a vortex-lattice model of the lifting surfaces.

The wing and flaps are divided into area elements, in each of which is placed a horseshoe vortex. Its bound leg is aligned with the element quarter chord and its trailing legs lie along the sides of the element as illustrated in figure 2. The trailing legs are positioned in the plane of their originating element, and they are deflected so that they lie in the plane of each surface downstream of the originating surface. The trailing legs extend to infinity in the plane of the last surface contacted.

The boundary conditions, expressing the flow tangency to the camber surface, are satisfied at a set of control points located at the midspan of the three-quarter chord line of each area element. The wing control points are all assumed to lie in the plane containing the root chord and making an angle $\phi$ with the $Z = 0$ plane. The control points on each flap are assumed to lie in the chord plane of the flap. The boundary condition equations (ref. 1) state that the total flow is tangent to the camber surfaces of the wing and flaps at each control point. The total velocity at each control point is made up of the free stream, the velocity induced by the vortex-lattice horseshoe vortex system, and additional velocities induced by an external source of disturbance. The solution of these equations provides the unknown value of the circulation of each horseshoe vortex.

Once the circulation strengths are determined, the flow field surrounding the lifting surface can be computed as well as the surface load distributions. The force on each area element is calculated as the product of density, local velocity normal to the element of vorticity, and circulation strength. The total force on each area element is made up of two contributions: that acting on the bound leg of the horseshoe vortex and the force acting on the trailing legs contained within the area element. There is only one bound leg associated with each area element, but numerous trailing legs may be present along each side of the area element, one for each area element upstream of the element being considered. All three components of force on each vortex leg are computed on each area element. These are resolved into normal and axial forces in each area element. The section characteristics of each lifting surface are computed from these elemental forces and finally the total individual surface forces are resolved into the gross aerodynamic characteristics relative to the aircraft axis system.

The vortex-lattice method is restricted to calculating longitudinal characteristics, and compressibility corrections are not included in the method. No small angle assumptions are used in the theoretical model.

Since the EBF model is to be used as a predictive technique, it is important that the vortex-lattice method be applicable to typical EBF configurations. The wing and flap configuration parameters are listed as follows:

Wing

Leading-edge shape: May have up to 30 breaks in sweep.

Trailing-edge shape: Same as leading edge.

Taper: Determined from leading-edge and trailing-edge specification.

Tip chord: Parallel to root chord.

Dihedral: Constant over the semispan.

Mean camber surface: May have both twist and camber.

Thickness: Neglected.

Flaps

Number: Up to ten individual flap segments.

Location: Only trailing-edge flaps are considered; gaps between surfaces are permitted.

Leading-edge shape: Straight.

Trailing-edge shape: Straight.

Taper: Linear.

Root chord: Must lie in a vertical plane parallel to the wing root chord.

Tip chord: Parallel to root chord.

Span: Full or partial span.

Deflection: Different for each flap.

Mean camber surface: Each flap may have both camber and twist.

Thickness: Neglected.

The vortex-lattice arrangement on each lifting surface is general enough to provide good flexibility in describing the loading distribution. A maximum of thirty (30) spanwise rows of vortices may be used, and each lifting-surface component can have a maximum of ten (10) chordwise vortices. The area elements on a lifting surface have the same chord at each spanwise station, but the element chords need not be the same on adjacent surfaces. Thus, the number of chordwise elements on each lifting surface may be chosen according to the accuracy required in the predicted chordwise loading distribution. In the spanwise direction, the widths of the area elements may be varied to fit the loading situations; that is, in regions of large spanwise loading gradients, the element widths may be reduced to allow closer spacing and more detailed load predictions. Convergence of predicted results as a function of lattice arrangement on wings and flaps is described in Appendix A of reference 2. One restriction on the spanwise lattice arrangement on the wing and flaps is the requirement that the lattice elements on the flaps be directly aligned with those on the wing. This requirement is imposed because of the deflection of the vortex trailing legs and the necessity for all trailing legs to lie along the edges of area elements.

When a wing-flap configuration has multiple spanwise flap segments with different deflection angles like that shown in figure 2, certain difficulties arise in calculating the loading distributions on the flap segments, particularly near the flap edges. The problem is caused by the deflected trailing legs from the upstream area elements on the wing. The individual circulation strengths can be large; but when the side edges of the area elements coincide, the trailing vortex legs tend to cancel and the net strength of the trailing vorticity on this side edge is quite small. When the side edges do not coincide, as is the case on adjacent flaps with different deflections, the net strength of the trailing legs along these edges can be large. This has two effects on the loading calculation. First, the unbalanced trailing leg strengths can cause unrealistic circulations to be computed near the flap edges; and because of the mutual interference between panels, this can be felt on surrounding panels. Second, these circulation distributions on the flaps lead to unusual force distributions. This particular problem is not

unique with this author as Rubbert presents an extensive investigation of the same type of difficulty in reference 3.

Since this problem has a large effect only on the flap loads on the area elements near the edges of the flaps, and the total effect on the gross loading on the configuration is small, the following approximate solution is applied to this area. The wing trailing vorticity at the semispan station corresponding to the flap side edges is not allowed to deflect along the flaps but is arbitrarily forced to move aft in the plane of the wing. It is relatively unimportant as to the exact position assigned to the wing trailing legs so long as they are combined; therefore, the choice was made to leave the wing trailing legs (at this one semispan station only) undeflected. There is still an imbalance in the trailing legs associated with the flap edges, but it generally has only a small effect on the resulting flap circulation distribution. In addition to the modification to the wing trailing leg positions, the imbalance in the trailing vortex strength on the flap edges produced some large forces on the flap edges. For this reason, it was necessary to neglect the normal-force component due to the trailing vortex leg at the free edge of each flap. These modifications smoothed the predicted load distribution on the flaps with negligible effect on the total loading on the configuration.

## Vortex Ring Jet Model

A potential flow model of a high-bypass-ratio turbofan engine wake is needed which will provide a means for calculating the induced velocity field both inside and outside the boundary of the jet wake. The flow model should simulate the entrainment effect exhibited by jet wakes, the jet boundaries should behave according to observed spreading rates for jets in a coflowing stream, and the wake should be positioned under the influence of a lifting surface such that it lies along a streamline. Such a potential flow model of a jet wake with circular cross section is presented in reference 2, and the flow model is extended to elliptic cross-sectional jets in reference 1.

The flow model consists of a distribution of vorticity placed on the surface of an expanding cylinder with circular or elliptical cross section. The strength of the vorticity is determined by the jet thrust coefficient. The distribution of vorticity on the cylinder is modeled by a series of vortex rings coaxial with the jet centerline and having the same cross-sectional shape as the cylinder. Each ring represents a finite increment of length of the cylinder, and the vortex strength of each individual ring is equal to the net vorticity on the incremental length of cylinder which it replaces. The momentum inside the jet boundary remains constant; and if the expansion of the boundary is specified correctly, the mass flow inside the boundary is in good

agreement with actual jets. Thus, the model represents the momentum, mass, and entrainment characteristics of a turbulent, coflowing jet. While the velocity profile within the jet is approximated by a uniform profile (fig. 3), the induced velocities outside the jet boundary are accurate because they are related to the entrainment induced flow.

Measured velocity profiles in the wake of a JT15D-1 jet engine mounted beneath a wing are available in reference 4. The profiles were measured on both the wing side and the free side of the engine centerline at a point approximately two nozzle diameters downstream of the engine exit. These data are shown in figure 4 for $C_T = 0.56$. A circular vortex ring jet model was designed to expand at a rate that would produce the same mass flow at the measured profile station. The resulting predicted velocity profile is also shown in figure 4. The jet model has approximately 5 percent less momentum than the real jet; therefore, the vortex ring model can satisfactorily match both mass and momentum of an actual jet if the correct spreading rate is known. Any interference calculation taking place inside the jet boundaries will be reasonably accurate when averaged over the total wake area, but there may be certain inaccuracies locally due to differences in the shape of the velocity profile within the wake.

Use of the vortex ring jet model requires three items to determine completely the analytical description of the jet. The first item is the initial vortex ring strength which is related to the thrust and momentum in the jet. The remaining two items are the boundary of the jet and the position of the jet centerline. The jet centerline can either be located a priori, or it can be left free to move under the influences of the free-stream velocity, the wing and flap loading induced flow field, and the jet induced flow field. The objective in permitting the centerline to move freely is to be able to position it along the streamline of the wing-flap-jet flow which leaves the center of the exhaust. Iterations can be performed until convergence is attained between the jet centerline and the streamline position.

To complete the description of the jet wake, the boundary of the jet must be specified at all points along the jet. An analytical method is available in reference 5 which gives the radius distributions for axisymmetric jets in a coflowing stream for various velocity ratios. Unfortunately, a similar series of curves is not available for noncircular cross-sectional jets. It is here that empirical evidence must be used to complete the specifications of the jet.

Little data exist on the cross-sectional shape of nonaxisymmetric jets in a coflowing stream. Jet wake extent and profiles measured aft of the last flap on a four-engine EBF configuration are presented in reference 6. These data illustrate that

initially circular jets tend to mix and become elliptical in cross section after interaction with the flaps. The expansion characteristics of these jets between the engine exit and the station aft of the wing is undetermined. Modeling of the jet in this region requires simply a good engineering estimate until more detailed measurements become available.

## Interference Calculation

Calculation of the aerodynamic loading of a wing-flap configuration under the influence of the jet wake of a turbofan engine is done with the combination of the two potential flow models described above. The two flow models are combined by superposition (fig. 5). The jet model induces a velocity field on the wing and flap which produces an interference loading on the lifting surfaces. The wing and flap loadings induce a velocity field in the vicinity of the jet and tend to deflect the jet away from these surfaces. It is assumed that the engine thrust is unaffected by the presence of the wing-flap. Because of the mutual interaction between the jet and lifting surfaces, an iterative solution is required. The solution is carried out in the following manner.

Before any calculations are made, the jet centerline is positioned with respect to the wing and flap. The initial location of the centerline can be based on some a priori knowledge of the flow field beneath the wing and flap system, or it can be located in a strictly arbitrary fashion. For example, it is quite acceptable to choose the initial jet centerline to be a straight line aft from the engine exhaust as illustrated in figure 5.

The (expanding) jet boundary and cross-sectional shape distribution should be chosen according to whatever procedure seems most appropriate, and this distribution (which will be unchanged from this point on) is placed on the centerline to define an initial jet wake. The jet-induced velocity field is computed at selected control points on the lifting surfaces and the circulation distribution on the wing and flaps is obtained such that the tangency boundary condition is satisfied at each control point.

At this point in the solution, the boundary condition on the wing and flap surfaces is satisfied but the jet position has not been influenced by the presence of the wing and flap. The wing-flap influence consists of modifying the jet location to cause the jet centerline to lie along a streamline of the combined jet-wing-flap flow. The initial jet centerline is adjusted by computing the total flow field at a number of points on the centerline and moving the centerline to a new position such that it lies along the computed flow direction at the specified points.

This completes the first iteration. In this situation, the wing and flap loading is not compatible with the jet flow field corresponding to the new position of the jet. Thus, a second iteration is needed.

The flow field corresponding to the adjusted jet position is computed, and a new wing-flap loading distribution is obtained. The jet centerline is again moved to lie along the new flow directions. This procedure is continued until either the centerline position or the total wing and flap loading converges to within a desired tolerance. With a converged solution, the total flow is tangent to the wing and flap surfaces and the jet centerline lies along a streamline of the flow.

It is during the iteration procedure and the subsequent motion of the jet centerline that another bit of empiricism is used. The combination of the two potential flow models results in the deflection of the jet such that it passes beneath the wing and flap surfaces. A typical converged solution will show the maximum jet centerline deflection angle to be close to the maximum flap angle. Measurements indicate that the turning efficiency of a typical EBF configuration can drop as low as 0.75 at high flap angles. Consequently, a limit on jet deflection angle is imposed during the iteration process to more realistically model jet deflection for high flap deflection angles.

## RESULTS

The methods of analysis described in the previous section have been applied to a number of different EBF configurations under various flow conditions. Convergence characteristics of the iteration procedure are examined, and comparisons with experimental data are presented.

### Convergence Characteristics

For purposes of examining the convergence characteristics of the prediction method, the four-engine EBF configuration of references 4 and 7 was chosen. This large-scale model has a 25° swept wing with an aspect ratio of 7.28 and a taper ratio of 0.4. The trailing-edge flap system considered for the calculations consists of three full-span, slotted flaps. Two JT15D-1 turbofan engines are pylon mounted beneath each wing at $\eta = 0.25$ and 0.42. The lattice arrangement for this configuration is shown in figure 6. The initial assumption for the jet centerline in all cases is a straight line coincident with the engine centerline. The convergence studies are carried out for the flaps in a take-off position ($\delta_f = 0°/20°/40°$) and a configuration angle of attack of 18.5°.

Convergence of the total wing-flap normal-force coefficient is shown in figure 7 for thrust coefficients of 2.3 and 4.0. At the end of the fourth iteration, both cases have converged to within 7 percent. This convergence pattern has been observed on the same configuration at other angles of attack and on other similar configurations.

The convergence of the normal-force coefficient on each component of the wing-flap configuration is shown in figure 8. Each component tends to converge according to its own pattern, but all components reach convergence at about the same time.

The convergence pattern of the spanwise distribution of section normal force on a single component, flap 2, of the configuration is shown in figure 9 through four iterations. The peak loadings are caused by direct jet interaction with the flap. The span loads on the other components have a similar convergence pattern and these are presented and discussed in reference 1.

The convergence results just described are typical of those observed on other EBF configurations over a wide range of flow conditions. The method has never failed to converge, but convergence is slower for high flap angles. Generally, calculations have been initiated with a straight jet centerline because of the simplicity in prescribing the input; however, the number of iterations required for convergence can be reduced if the initial centerline is located closer to the final position. On the basis of cases run, convergence is more rapid if the centerline approaches its final position from above rather than below, because the correcting velocities causing the centerline position to change are larger if the centerline starts too close to the wing and flaps.

## EBF Data Comparisons

The overall EBF prediction method was evaluated by comparing predicted results with data on several EBF configurations. These comparisons are presented and discussed in detail in reference 1, and results presented herein are typical examples of those included in that reference.

The first configuration to be considered is the four-engine model of references 4 and 7 with take-off flap setting ($\delta_f = 0^\circ/20^\circ/40^\circ$). The jet turning efficiency was assumed to be 85 percent which limited the jet downward deflection angle to $34^\circ$ for all calculations. The predictions to follow have all converged to within an 8-percent tolerance. The convergence is not the same at all angles of attack, thus introducing some uncertainty in the slope of the predicted curves.

In figure 10, the predicted section normal-force coefficient on flaps 1, 2, and 3 are compared with experimental results at $C_\mu = 4$ and $\alpha = 18.5^\circ$ obtained from reference 7. Wing data are not available for this configuration. The predicted peak loadings on flaps 1 and 2 are greater than those measured and cover a smaller portion of the wing. This indicates that the chosen jet model has not expanded sufficiently at this station and perhaps should be expanded at a faster rate to produce better agreement with experiment. As noted on the figure, the predicted total normal-force coefficients on flaps 1 and 2 are larger than the value obtained by integrating the measured distribution. The comparison for flap 3 in this same figure shows good agreement between the predicted and measured loading distributions. The peak loadings, the width of the loading, and the total normal force on the flap are all in good agreement. Since this flap is nearest to the point at which the jet wake is specified, based on measurements in the wake of a similar EBF configuration (ref. 6), the jet model is probably in better agreement with the actual jet on this flap than on the previous two flaps.

The predicted and measured longitudinal aerodynamic coefficients on the four-engine EBF model with take-off flap configuration are compared in figure 11. The predicted curves include estimates for the force and moment contributions due to the fuselage and engines. No estimate of viscous drag is included in the predicted drag curve. The power-on results indicate that the method is converging on a lift coefficient that is too low at low angles of attack. This result may be caused by a poor estimate for the jet turning efficiency. The predicted pitching-moment coefficients are in reasonable agreement with experiment, but the moment curve slopes are in error. The predicted drag curves are in good agreement with experiment.

Comparisons of the measured and predicted section normal-force coefficients on the same wing with landing flap configuration ($\delta_f = 15^\circ/35^\circ/55^\circ$) are shown in figure 12 for $C_\mu = 4$ and $\alpha = 6.5^\circ$. The high loading peaks on the wing are caused by the jet being driven up against the aft portion of the wing by the induced upwash from the high loading on the flaps. The loading peaks are also narrow compared to the data, another indication that the real jet may be spreading faster than the assumed analytical model. The loading peaks and spanwise extent of the jet-induced loading on the flaps are in reasonable agreement as illustrated in the remainder of figure 12.

The measured and predicted longitudinal aerodynamic coefficients on the landing flap configuration are compared in figure 13. The overall results are very similar to those presented for the take-off configuration. These results were obtained assuming jet turning efficiency of approximately 0.70; thus, the jet turning angle was limited to a maximum downward deflection of $38.5^\circ$.

The predicted flow field aft of the trailing edge of the last flap at a spanwise station corresponding to the centerline of the inboard jet is shown in figure 14 for the take-off configuration ($\delta_f = 0°/20°/40°$) at $C_\mu = 2.3$ and $\alpha = 18.5°$. The uniformity of the jet flow characteristics of the vortex ring model is well illustrated. In the inset, the measured flow field aft of a similar EBF configuration under similar flow conditions is reproduced from reference 6. The measured flow field, also aligned with the centerline of the inboard jet, is very much like the predicted flow field.

The results presented thus far have all been obtained using a circular cross-sectional jet model because adequate information needed to specify an elliptic jet boundary are not available. Some results obtained using the elliptic jet model are described in reference 1. The elliptic jet used had the same initial momentum and cross-sectional area distribution along the centerline as the circular jet model. The elliptic jet was assumed to expand linearly from a circular cross section at the engine exit to a 2:1 ellipse aft of the last flap. The same jet turning efficiency used for the circular jet model was retained. The calculation was carried out for the landing flap configuration at $\alpha = 18.5°$ with the following results. The predicted loading is distributed differently over the wing and flap surfaces due to the different cross-sectional shape of the two jets, but the total normal force imparted to the wing-flap configuration by the elliptic jet model is only 2 percent different from that obtained from the circular jet model. It appears that the cross-sectional shape of the jet is important if loading distributions are important; but if gross aerodynamic forces are the goal of the calculation, the jet cross-sectional shape is relatively unimportant so long as the momentum in the jet is correct.

## CONCLUDING REMARKS

An engineering prediction method developed to predict the loading distributions and longitudinal aerodynamic characteristics of externally blown flap configurations has been described. Comparisons of measured and predicted gross lift, drag, and pitching-moment coefficients on configurations with moderate flap angles ($\delta_f \leq 40°$) indicate generally good agreement for all thrust levels. This is due principally to the correct modeling of the entrainment and momentum characteristics of the engine wakes and to the proper treatment of the mutual interference between the jet wake and wing-flap. The interference model creates, on the wing-flap, both the momentum reaction due to jet deflection and the additional induced circulation characteristic of EBF systems.

As the flap angles increase beyond 40°, the predicted results agree less well with the data. The assumption that the wing-flap induced interference on the jet affects only its centerline and not its boundary becomes less accurate as the jet is more highly deformed, and it is possible that this is responsible for the poorer agreement at the higher flap angles.

Comparisons of measured and predicted spanwise loading distributions on the individual lifting surfaces indicate good quantitative agreement in some cases and poor agreement in others. Generally, the correct qualitative behavior is predicted in which large peak loadings occur locally on the flaps due to direct impingement of the jet wakes, but the magnitude of the peaks is not consistently in good agreement with the data. The differences are felt to be due primarily to the modeling of the velocity profile within the wake and the boundary of the wake.

## REFERENCES


1. Mendenhall, M. R., Spangler, S. B., Nielsen, J. N., and Goodwin, F. K.: Calculation of the Longitudinal Aerodynamic Characteristics of Wing-Flap Configurations With Externally Blown Flaps. NEAR TR 97, Dec. 1975. NASA CR-2705, 1976.

2. Dillenius, M. F. E., Mendenhall, M. R., and Spangler, S. B.: Calculation of the Longitudinal Aerodynamic Characteristics of STOL Aircraft with Externally-Blown Jet-Augmented Flaps. NASA CR-2358, Feb. 1974.

3. Rubbert, P. E.: Theoretical Characteristics of Arbitrary Wings by a Non-Planar Vortex Lattice Method. Boeing Rept. D6-9244, Feb. 1964.

4. Aoyagi, K., Falarski, M. D., and Koenig, D. G.: Wind-Tunnel Investigation of a Large-Scale 25° Swept-Wing Jet Transport Model with an External Blowing Triple-Slotted Flap. NASA TM X-62,197, Nov. 1973.

5. Abramovich, G. N.: The Theory of Turbulent Jets. MIT Press, 1963.

6. Johnson, W. G., Jr. and Kardas, G. E.: A Wind-Tunnel Investigation of the Wake Near The Trailing Edge of a Deflected Externally Blown Flap. NASA TM X-3079, Oct. 1974.

7. Perry, B., III and Greene, G. C.: Wind-Tunnel Investigation of Aerodynamic Loads on a Large-Scale Externally Blown Flap Model and Comparison with Theory. NASA TN D-7863, Mar. 1975.

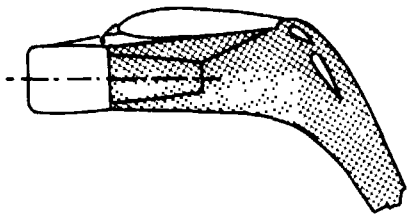

Figure 1.- EBF configuration.

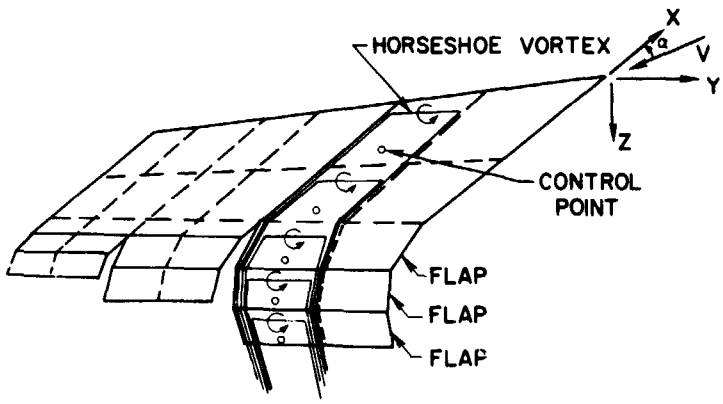


Figure 2.- Wing-flap vortex-lattice model.

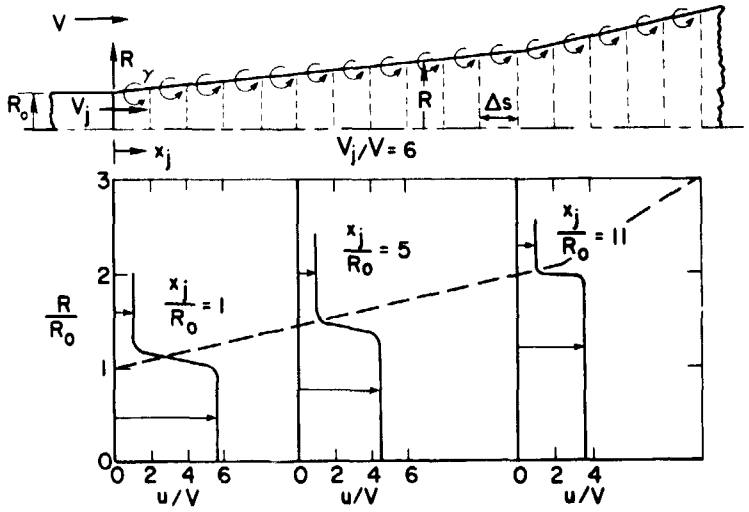


Figure 3.- Circular vortex ring wake model and velocity profiles.

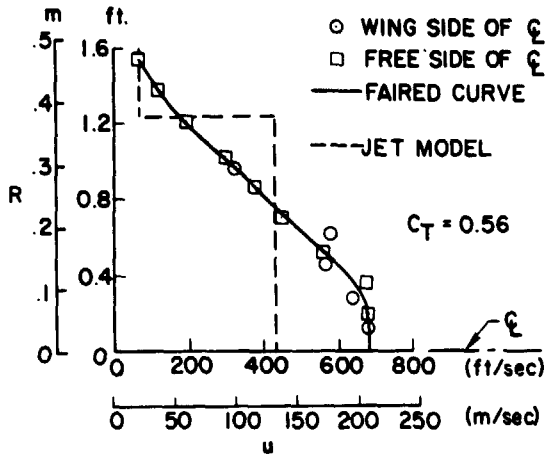


Figure 4.- Measured and predicted velocity profiles in the wake of a JT15D-1 jet engine.

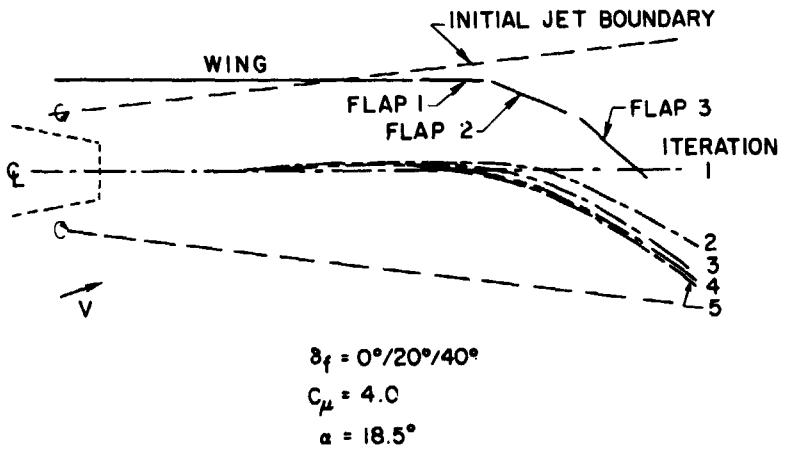


Figure 5.- Convergence of inboard jet centerline on a four-engine EBF configuration.

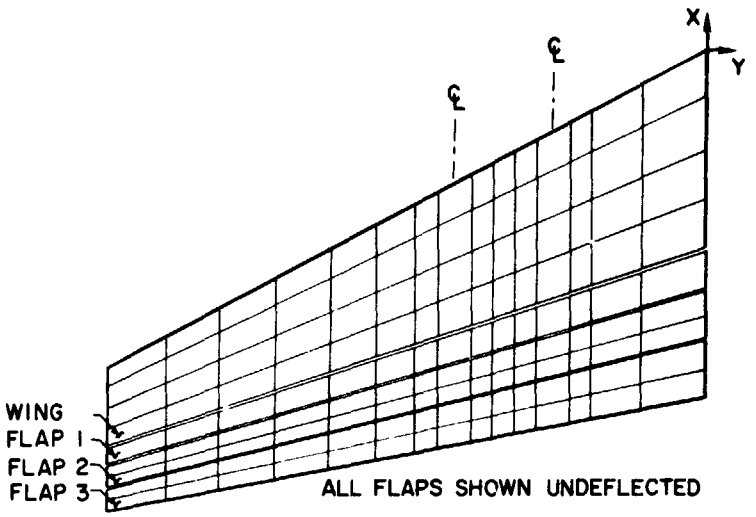


Figure 6.- Vortex-lattice arrangement for EBF configuration.

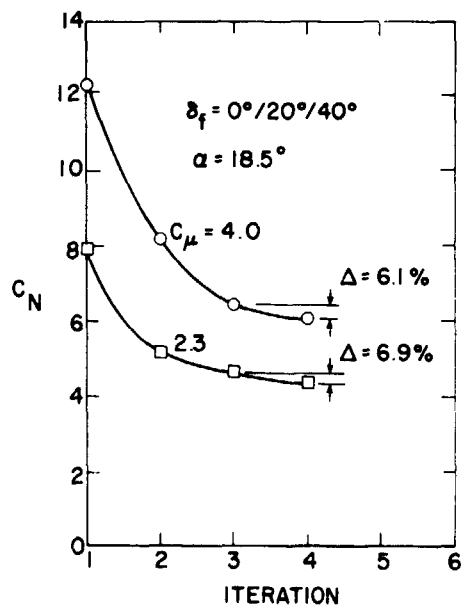


Figure 7.- Convergence of the total wing-flap normal-force coefficient on a four-engine EBF configuration.

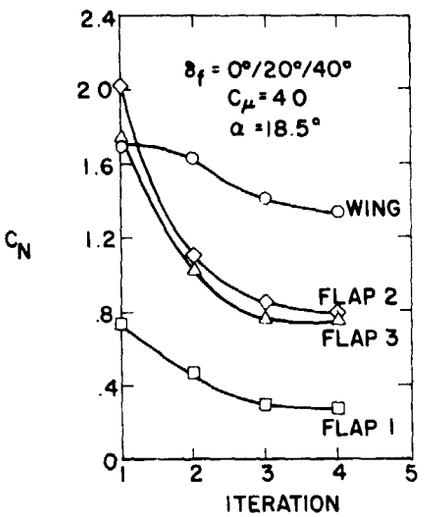


Figure 8.- Convergence of normal-force coefficients on the wing and flaps of a four-engine EBF configuration.

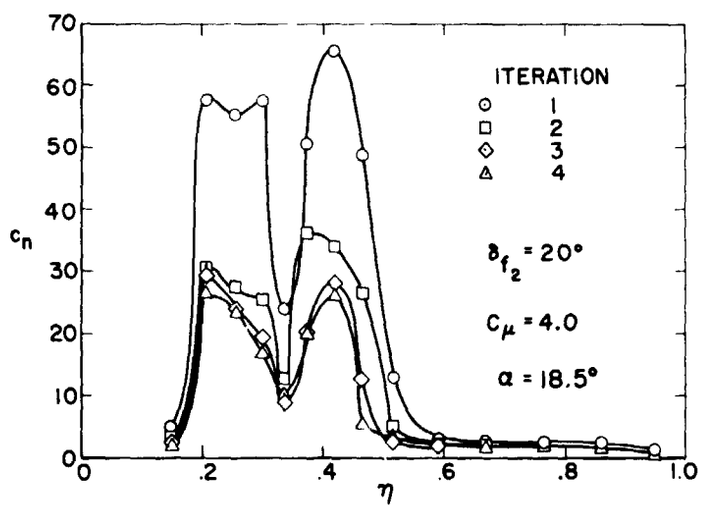


Figure 9.- Convergence of predicted spanwise distribution of section normal-force coefficients on flap 2 of a four-engine EBF configuration.

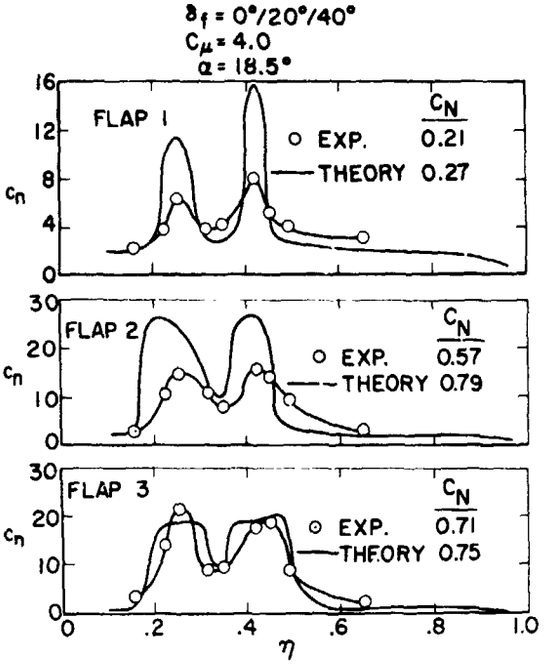


Figure 10.- Measured and predicted section normal-force coefficients on the lifting surfaces of a four-engine EBF model.

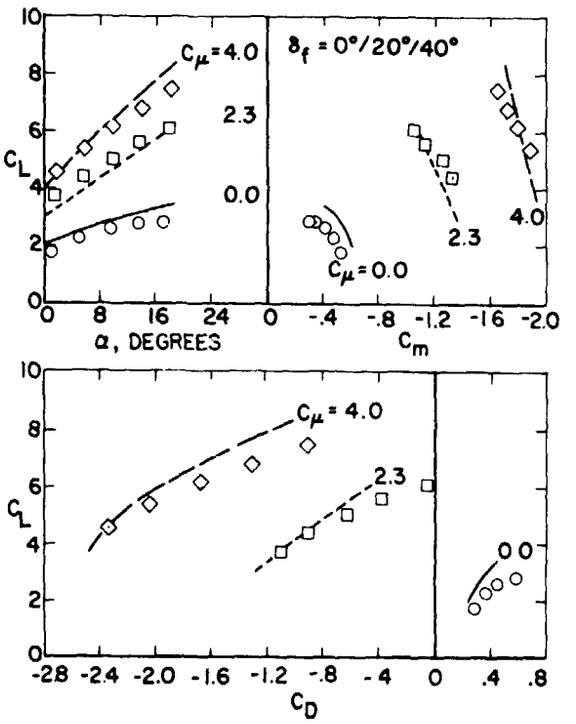


Figure 11.- Measured and predicted longitudinal aerodynamic characteristics of a four-engine EBF configuration.

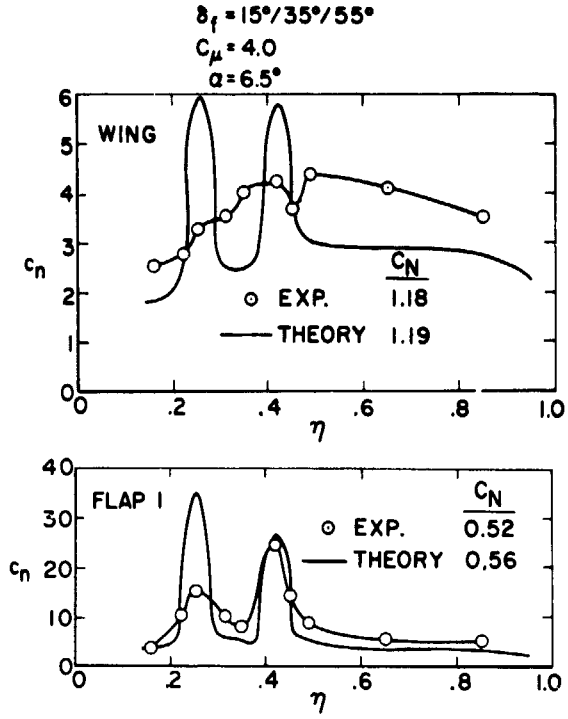


Figure 12.- Measured and predicted section normal-force coefficients on the lifting surfaces of a four-engine EBF configuration.

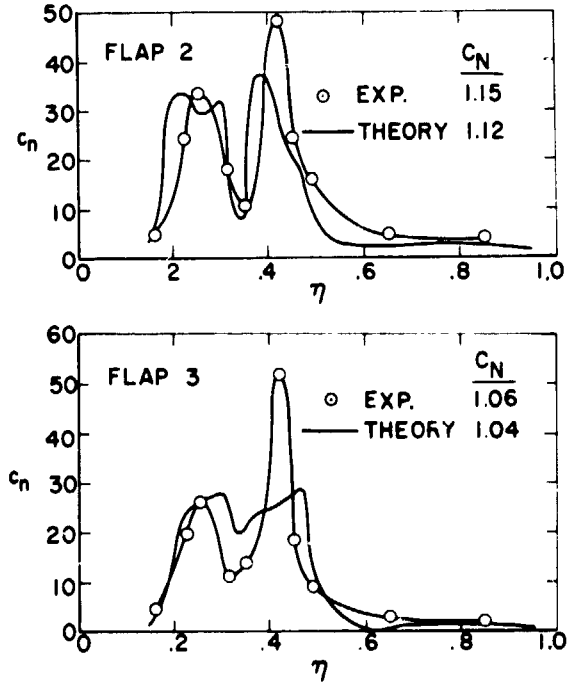


Figure 12.- Concluded.

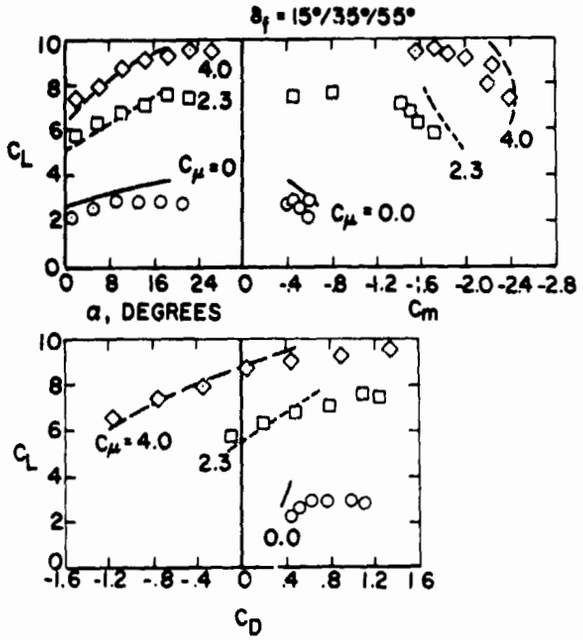


Figure 13.- Measured and predicted longitudinal aerodynamic characteristics of a four-engine EBF configuration.

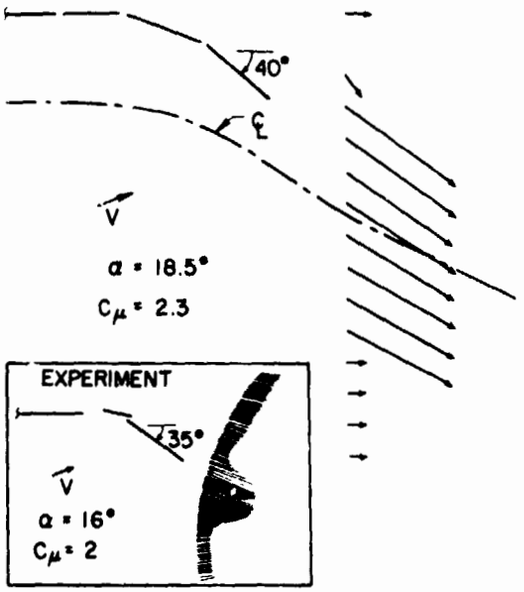


Figure 14.- Measured and predicted flow fields aft of EBF configurations.